

# Massive Synchrony in Distributed Antenna Systems

Erik G. Larsson

**Abstract**—Distributed antennas must be phase-calibrated (phase-synchronized) for certain operations, such as reciprocity-based joint coherent downlink beamforming, to work. We use rigorous signal processing tools to analyze the accuracy of calibration protocols that are based on over-the-air measurements between antennas, with a focus on scalability aspects for large systems. We show that (i) for some who-measures-on-whom topologies, the errors in the calibration process are unbounded when the network grows; and (ii) despite that conclusion, it is optimal – irrespective of the topology – to solve a single calibration problem for the entire system and use the result everywhere to support the beamforming. The analyses are exemplified by investigating specific topologies, including lines, rings, and two-dimensional surfaces.

**Index Terms**—phase calibration, synchronization, reciprocity, distributed antennas, MIMO, estimation, graph models, scalability

## I. INTRODUCTION

A distributed antenna system consists of access points that are spread out geographically and cooperate phase-coherently on wireless communication or sensing tasks. This concept is considered a main technology component of the 6G physical layer, and variations of it appear under the names *distributed multiple-input multiple-output (MIMO)* [1], *network MIMO* [2], *user-centric MIMO* [3], *cell-free massive MIMO* [4], *RadioWeaves* [5], and *radio stripes* [6]. Each access point may have a single service antenna, or an array (panel) of antennas.

At any point in time, each [service] antenna,  $n$ , is associated with two complex-valued coefficients,  $T_n$  and  $R_n$ , that account for hardware imperfections and oscillator synchronization errors, and which multiply the transmitted and received complex-baseband signals. Herein, we will only be concerned with phase and set, for the  $n$ th antenna,  $T_n = e^{-jt_n}$  and  $R_n = e^{jr_n}$  for some phase values  $t_n$  and  $r_n$ , defined mod  $2\pi$ . The convention with a minus sign on  $t_n$  facilitates an interpretation of  $\{t_n, r_n\}$  in terms of time-delays [7]. The phase values  $\{t_n, r_n\}$  collectively model two separate effects:

E1. Geographically separated access points may have their own local oscillators that drive their radio-frequency mixers. These oscillators are imperfect and noisy, and they differ from their nominal specifications. This results in a time-varying shift between the oscillator phases at different access points. Unless all oscillators are locked to a common reference using a synchronization cable – which is costly and even infeasible in some deployment scenarios – this phase shift can fluctuate and grow quickly.

The author is with Linköping University, Dept. of Electrical Engineering (ISY), 581 83 Linköping, Sweden. E-mail: erik.g.larsson@liu.se. This work was supported by ELLIT, the KAW Foundation, the Swedish Research Council (VR), and the REINDEER project of the European Union’s Horizon 2020 research and innovation program under grant agreement No. 101013425.

E2. The transmit and receive electronics branch at every antenna will have an unknown phase lag that depends on manufacturing variations and imperfections in the circuits. This lag varies also varies with time, but slowly, once the equipment has warmed up. The exact time constant of the variation depends on the actual hardware; in experimental work reported in [8], the phase was substantially constant for hours.

### A. Calibration Over-the-Air

Knowledge of certain relations between  $\{t_n, r_n\}$  is essential for the antennas to cooperate phase-coherently. That calls for calibration in order to periodically estimate these values, or appropriate functions thereof. We will be concerned with calibration based on *over-the-air measurements* (in situ) between pairs of antennas. Within an access point one relies on coupling among the antennas; between access points, one relies on radio-frequency propagation. Calibration within an access point may alternatively be aided by dedicated internal calibration loops [9], [10], but that will be of no further concern here.

Our analysis herein will be agnostic to the actual origin of the variations in  $\{t_n, r_n\}$ , and to whether different antennas are co-located in an array or geographically separated. But we emphasize that in practice, E1 presents a much greater challenge than E2, especially if the oscillators are not locked to a common reference. Also, in practice, in a system with geographically separated multiple-antenna access points it can be advantageous to separate the problems of calibrating for E1 and E2: calibrate the antennas within an access point infrequently, and between the access points more frequently.<sup>1</sup>

### B. Different Types of Calibration

Distributed antenna systems can operate with different purposes, requiring different types of calibration [7]. Of particular interest are reciprocity (R) calibration, and full (F) calibration. Here we give a concise exposition, to provide context.

1) *Reciprocity (R) calibration*: The system is R-calibrated if  $\{t_n + r_n\}$  are known, mod  $2\pi$ , up to a common constant for all  $n$ . R-calibration enables reciprocity-based, joint coherent operation, relying on uplink pilots for downlink multiuser MIMO beamforming. Over-the-air methods for R-calibration use bidirectional measurements between antennas, essentially measuring  $(t_n + r_n) - (t_{n'} + r_{n'})$  for different pairs  $(n, n')$ . This can be done for both co-located arrays [8], [11]–[19] and for distributed antenna systems [20]–[27].

Importantly, over-the-air R-calibration works without knowing a priori the propagation delay (coupling) between antennas.

<sup>1</sup>Alternative terms for [phase] calibration between access points are *phase synchronization* and *phase alignment*. Herein, we use the term *calibration*.

Therefore, there is no difference in principle between R-calibrating the antennas in a single co-located array and [jointly] R-calibrating all antennas in a distributed antenna system – other than that in the presence of oscillator drifts, a distributed system would have to be re-calibrated more often. (The main effect in this case is E1; for more discussion of the need for re-calibration in the presence of oscillator drifts, see [7], [28].)

It is important to appreciate the distinction between *channel estimation* and (R-)calibration. Both are required for joint coherent, reciprocity-based downlink beamforming to work. While channel estimation in multiple-antenna systems is well researched [3], the calibration problem has received less attention. Yet, the latter is a difficult problem. In time-division duplexing (TDD) operation, channel estimates can be obtained, to any desired degree of accuracy, by sending uplink pilots with appropriate length, power, and reuse patterns. But over-the-air phase calibration requires the transmission of specially designed signals *between* service antennas, which breaks the TDD flow.

2) *Full (F) calibration*: The system is F-calibrated if  $\{r_n - r_{n'}\}$ ,  $\{t_n - t_{n'}\}$  and  $\{r_n - t_n\}$  are known, mod  $2\pi$ , for all  $(n, n')$ . Variations exist, for F-calibration only on receive or transmit. F-calibration is stronger than R-calibration, and enables the use of geometrically parameterized array models – facilitating fingerprinting and directional (in angle) beamforming. F-calibration implies R-calibration, but not conversely.

F-calibration can also be performed over-the-air by performing measurements between antennas [29], [30], but this requires the propagation delay between the antennas to be a priori known [7] – which can be challenging in a distributed antenna system.

### C. Specialization to R-Calibration

In the rest of the paper we consider only R-calibration, although some of the results also apply, *mutatis mutandis*, to other types of calibration. We define, for each antenna  $n$ , the phase parameter  $\phi_n = t_n + r_n$ . The calibration objective is then to obtain estimates,  $\{\hat{\phi}_n\}$ , of  $\{\phi_n\}$ , from pairwise measurements between antennas. We call  $\{\hat{\phi}_n - \phi_n\}$  the [phase] estimation errors.

In what follows, by system *topology* we refer to the graph that defines who measures on whom – not to be confounded with how antennas are interconnected over backhaul, which is unimportant here.

### D. Contributions and Preview of the Results

The contribution of this paper is a rigorous analysis of over-the-air calibration, specifically addressing three questions:

Q1. How accurately can  $\{\phi_n\}$  be estimated, for different system topologies? Let  $N$  be the total number of antennas in the system. What happens when  $N$  increases: does the calibration problem become easier or harder?

We show that for some topologies,  $\text{Var}\{\hat{\phi}_n\}$  can grow unbounded, for all  $n$ . This happens, for example, for the line (radio stripe) topology in Figure 1, where antennas measure only on their immediate neighbors (Section V-A).

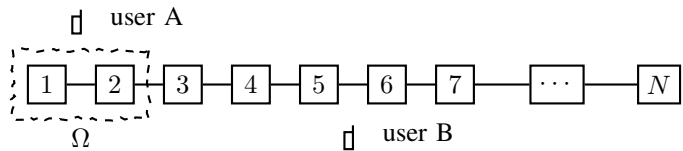


Fig. 1. Line topology, where antennas perform calibration measurements on their immediate neighbors. Two users A and B are also shown.

Note that  $\{\phi_n\}$ , of course, are bounded as they are only defined mod  $2\pi$ , so this asymptotic statement means that errors aggregate unfavorably.

Q2. When performing reciprocity-based beamforming to a user, from a *subset* – to be denoted  $\Omega$  – of the antennas, how should calibration be performed? One may either (a) perform R-calibration problem for the whole system, or (b) perform R-calibration only involving the subset  $\Omega$ . For example, consider Figure 1: user A is in the field-of-view of antennas 1 and 2; user B is in the field-of-view of antennas 5 and 6. When calibrating for beamforming to A, will it be advantageous to (a) use calibration measurements among all  $N$  antennas, or (b) involve only antennas 1 and 2 in the calibration?

From the answer to Q1, one may intuit that option (b) is preferable over (a). But we prove that (a) is always better: irrespective of the topology, it is optimal to solve a single calibration problem for the entire system (Section IV).

Q3. For what topologies is it possible to achieve *massive synchrony*, such that  $\{\text{Var}\{\hat{\phi}_n\}\}$  remain bounded, or even vanish, when  $N \rightarrow \infty$ ?

While a complete characterization remains open, we hope that our analysis offers a starting point (Section VI).

### E. Related Work

The most closely related work is the above-cited literature on R-calibration [7], [8], [11]–[27]. Note that despite its title, [20] does not consider the scalability aspects that we analyze herein.

Our results also have some connection to the writings on distributed synchronization in complex and wireless networks [31]–[36]. That literature, however, deals with protocols for synchronization by bilateral interaction between devices, whereas we consider calibration using centrally processed measurements.

### F. Notation

Lowercase bold symbols are column vectors, and uppercase bold symbols are matrices.  $(\cdot)^*$  represents the complex conjugate.  $\mathbf{0}$  is the all-zeros vector/matrix.  $\mathbf{I}$  is the identity matrix, and  $\{e_n\}$  denote the columns of  $\mathbf{I}$ . For a set  $\Omega$ ,  $\Omega^c$  denotes its complement. Given a set of integers,  $\Omega$ ,  $\mathbf{E}_\Omega$  denotes a matrix comprising the columns  $\{e_n : n \in \Omega\}$ .  $(\cdot)^T$  denotes the transpose of a vector or matrix, and  $(\cdot)^H$  denotes the Hermitian transpose.  $\mathbf{u}$  is the vector of all ones:  $\mathbf{u} = [1, \dots, 1]^T$ . For a vector  $\mathbf{x}$ ,  $\|\mathbf{x}\|$  is its norm. For a matrix  $\mathbf{X}$ ,  $\mathbf{X}^{-1}$  is its inverse,  $\det(\mathbf{X})$  is its determinant, and  $[\mathbf{X}]_{kl}$  is its  $(k, l)$  element. For

a positive semidefinite matrix  $\mathbf{X}$ ,  $\mathbf{X}^{1/2}$  denotes its positive semidefinite matrix square root. For symmetric matrices  $\mathbf{X}$  and  $\mathbf{Y}$  of compatible dimensions,  $\mathbf{X} \succcurlyeq \mathbf{Y}$  means that  $\mathbf{X} - \mathbf{Y}$  is positive semidefinite.

## II. ESTIMATING $\{\phi_n\}$ FROM MEASUREMENTS

### A. Calibration Measurement Model

All phase values are defined mod  $2\pi$ . We will assume that  $|\phi_n - \phi_{n'}|$  is small for all pairs  $(n, n')$ , so that we can ignore the mod  $2\pi$  operation when differences between phase values are of concern. For R-calibration specifically, this means that  $\{t_n + r_n\}$  differ only slightly for different  $n$ , such that the calibration only aims at correcting small residual errors; for example, this is the case if a coarse calibration has been undertaken previously.

The  $N$  antennas perform bidirectional over-the-air calibration measurements on one another. Each pairwise interaction, say between antennas  $n$  and  $n'$ , results in a measurement of  $\phi_n - \phi_{n'}$ , mod  $2\pi$ . If antennas  $n_m$  and  $n'_m$  intercommunicate in the  $m$ th measurement, this measurement is,

$$x_m = \phi_{n_m} - \phi_{n'_m} + w_m, \quad (1)$$

where  $w_m$  is noise. All differences  $\{\phi_n - \phi_{n'}\}$  are small, and defined mod  $2\pi$ ; so are  $\{x_m\}$ .

The calibration objective is to estimate  $\{\phi_1, \dots, \phi_N\}$  from  $\{x_1, \dots, x_M\}$ , where  $M$  is the number of measurements. This problem is ill-posed, irrespective of how large  $M$  is or of the topology: by adding an arbitrary constant to all  $\{\phi_n\}$ , none of  $\{x_m\}$  changes. However, with enough measurements, all  $\{\phi_n\}$  can be estimated up to a common, additive constant.

Throughout, the measurement noise is the only source of randomness, and all expectations are with respect to this noise. We assume that the measurement noises  $\{w_m\}$  are zero-mean random variables with a known positive definite covariance matrix,

$$\mathbf{Q} = \text{Cov}\{\mathbf{w}\}, \quad (2)$$

where  $\mathbf{w} = [w_1, \dots, w_M]^T$ .

In practice, one may explicitly perform pairwise measurements, as suggested by (1). Alternatively, one could have each antenna broadcast a synchronization pilot that is received by several neighboring antennas simultaneously. In this case, each bidirectional measurement is completed first when both involved nodes have performed their broadcast. For R-calibration of co-located arrays, such broadcasting strategies were developed in [18], [19]. Hereafter, the term ‘‘measurement’’ means an estimate of  $\phi_n - \phi_{n'}$  for an antenna pair  $(n, n')$ , irrespective of whether this estimate is obtained by a single, direct bidirectional measurement, averaging of multiple bidirectional measurements, or the use of a broadcast scheme.

### B. Graph Representation of the Measurement Model

We represent the measurement topology by an undirected graph  $\mathcal{G}$ , whose nodes represent the  $N$  antennas and whose edges represent the  $M$  measurements. Let  $\mathbf{B}$  be the  $M \times N$  incidence matrix of  $\mathcal{G}$ , whose  $m$ th row corresponds to

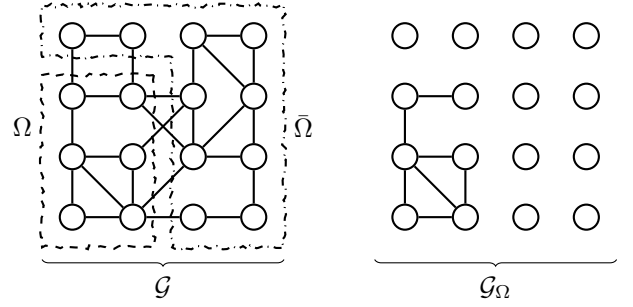


Fig. 2. Example of  $\mathcal{G}$ ,  $\mathcal{G}_\Omega$ ,  $\Omega$ , and  $\bar{\Omega}$ . Here  $N = 16$ ,  $N_\Omega = 6$ ,  $M = 25$  and  $M_\Omega = 7$ .

the  $m$ th edge of  $\mathcal{G}$  (the  $m$ th measurement). For each  $m$ ,  $[\mathbf{B}]_{mn_m} = 1$  and  $[\mathbf{B}]_{mn'_m} = -1$ . All other elements in the  $m$ th row of  $\mathbf{B}$  are zero. Furthermore, let  $\mathbf{x} = [x_1, \dots, x_M]^T$  and  $\boldsymbol{\phi} = [\phi_1, \dots, \phi_N]^T$ . Then

$$\mathbf{x} = \mathbf{B}\boldsymbol{\phi} + \mathbf{w}. \quad (3)$$

We define the pre-whitened measurement vector

$$\mathbf{x}' = \mathbf{Q}^{-1/2}\mathbf{x} = \mathbf{Q}^{-1/2}\mathbf{B}\boldsymbol{\phi} + \mathbf{w}', \quad (4)$$

in which the effective noise

$$\mathbf{w}' = \mathbf{Q}^{-1/2}\mathbf{w} \quad (5)$$

has covariance matrix  $\text{Cov}\{\mathbf{w}'\} = \mathbf{I}$ .

The two cases of interest are:

- All  $N$  antennas are involved in the calibration. In this case, we denote the graph by  $\mathcal{G}$  and its incidence matrix by  $\mathbf{B}$ , as already defined. The measurements are represented by the vector  $\mathbf{x}$  in (3), or equivalently, the pre-whitened vector  $\mathbf{x}'$  in (4).
- Only a subset,  $\Omega$ , of the antennas are involved in the calibration. The corresponding graph is a subgraph of  $\mathcal{G}$ , with  $N$  nodes and  $M_\Omega$  edges, where  $M_\Omega$  is the number of edges between nodes in  $\Omega$ . We denote this subgraph by  $\mathcal{G}_\Omega$ , and its  $M_\Omega \times N$  incidence matrix by  $\mathbf{B}_\Omega$ . Let  $\mathbf{x}_\Omega$  be the  $M_\Omega$ -vector comprising the measurements among the antennas in  $\Omega$ ; without loss of generality, we can assume that the  $M_\Omega$  last elements of  $\mathbf{x}$  contain  $\mathbf{x}_\Omega$ , such that  $\mathbf{x}_\Omega = [\mathbf{0} \ \mathbf{I}]\mathbf{x}$ . We denote the pre-whitened measurements by  $\mathbf{x}'_\Omega = \mathbf{Q}_\Omega^{-1/2}\mathbf{x}_\Omega$ , where

$$\mathbf{Q}_\Omega = \begin{bmatrix} \mathbf{0} & \mathbf{I} \end{bmatrix} \mathbf{Q} \begin{bmatrix} \mathbf{0} \\ \mathbf{I} \end{bmatrix} \quad (6)$$

is the  $M_\Omega \times M_\Omega$  lower-right corner of  $\mathbf{Q}$ , that is, the part of the noise covariance matrix associated with the  $M_\Omega$  measurements.

We assume that the nominal graph  $\mathcal{G}$  is connected. The graph  $\mathcal{G}_\Omega$  has  $N - N_\Omega$  isolated nodes, corresponding to antennas that do not participate. We assume that the part of  $\mathcal{G}_\Omega$  corresponding to the  $N_\Omega$  antennas that actually participate, is connected. Figure 2 shows an example.

The Laplacian of the nominal graph,  $\mathcal{G}$ , is  $\mathbf{B}^T \mathbf{B}$ . To accommodate a general noise covariance matrix we define the matrix

$$\mathbf{L} = \mathbf{B}^T \mathbf{Q}^{-1} \mathbf{B}. \quad (7)$$

If  $\mathbf{Q} = \mathbf{I}$ ,  $\mathbf{L}$  reduces to the standard graph Laplacian. If  $\mathbf{Q}$  is diagonal,  $\mathbf{L}$  becomes the Laplacian of a weighted graph (with weights equalling the reciprocal measurements variances). For general  $\mathbf{Q}$ , the matrix  $\mathbf{L}$  is not a conventional Laplacian matrix, but its nullspace is the same as that of the Laplacian  $\mathbf{B}^T \mathbf{B}$ , and this is what is required by the subsequent analysis.

Since  $\mathcal{G}$  is connected, the nullspace of  $\mathbf{B}^T \mathbf{B}$ , and therefore of  $\mathbf{L}$ , is one-dimensional and spanned by  $\mathbf{u}$  [37]. More specifically, by a basis change,  $\mathbf{L}$  can be written as,

$$\mathbf{L} = [\mathbf{u} \ \mathbf{Z}] \begin{bmatrix} 0 & \mathbf{0} \\ \mathbf{0} & \mathbf{\Lambda} \end{bmatrix} \begin{bmatrix} \mathbf{u}^T \\ \mathbf{Z}^T \end{bmatrix}, \quad (8)$$

where  $\mathbf{\Lambda}$  is an  $(N-1) \times (N-1)$  diagonal matrix whose (positive) diagonal elements are the non-zero eigenvalues of  $\mathbf{L}$ , and where  $\mathbf{Z}$  is an  $N \times (N-1)$  matrix whose columns are eigenvectors of  $\mathbf{L}$  and constitute an orthonormal basis for the orthogonal complement of  $\mathbf{u}$ . Note that (8) is similar to the eigenvalue decomposition, but not identical thereto as  $\mathbf{u}$  does not have unit norm.

The Laplacian of the weighted subgraph,  $\mathcal{G}_\Omega$ , is given by  $\mathbf{B}_\Omega^T \mathbf{B}_\Omega$ . Similarly to above, we define

$$\mathbf{L}_\Omega = \mathbf{B}_\Omega^T \mathbf{Q}_\Omega^{-1} \mathbf{B}_\Omega, \quad (9)$$

which again, is a (weighted) graph Laplacian if  $\mathbf{Q}$  is diagonal. The nullspace of  $\mathbf{L}_\Omega$  has dimension  $N_\Omega + 1$ . Through a basis change, we can write,

$$\mathbf{L}_\Omega = [\mathbf{u} \ \mathbf{E}_{\bar{\Omega}} \ \mathbf{Z}_\Omega] \begin{bmatrix} 0 & \mathbf{0} & \mathbf{0} \\ \mathbf{0} & \mathbf{0} & \mathbf{0} \\ \mathbf{0} & \mathbf{0} & \mathbf{\Lambda}_\Omega \end{bmatrix} \begin{bmatrix} \mathbf{u}^T \\ \mathbf{E}_{\bar{\Omega}}^T \\ \mathbf{Z}_\Omega^T \end{bmatrix}, \quad (10)$$

for some diagonal  $\mathbf{\Lambda}_\Omega$ , where  $\mathbf{Z}_\Omega$  is an  $N \times (N_\Omega - 1)$ -dimensional matrix whose columns constitute an orthonormal basis of the orthogonal complement of  $\{\mathbf{u}, \mathbf{E}_{\bar{\Omega}}\}$ . Note that (10) is not the eigenvalue decomposition, since (among others)  $\mathbf{u}$  and the columns of  $\mathbf{E}_{\bar{\Omega}}$  are not orthogonal.

For future use, we note the following facts:

- For  $\mathbf{Z}$ , it holds that

$$\mathbf{Z}^T \mathbf{u} = \mathbf{0}, \quad (11)$$

$$\mathbf{Z}^T \mathbf{Z} = \mathbf{I}, \quad (12)$$

$$\mathbf{Z} \mathbf{Z}^T = \mathbf{I} - \frac{1}{N} \mathbf{u} \mathbf{u}^T \quad (13)$$

$$\mathbf{Z}^T \mathbf{L} \mathbf{Z} = \mathbf{\Lambda}. \quad (14)$$

- For  $\mathbf{Z}_\Omega$ , it holds that

$$\mathbf{Z}_\Omega^T \mathbf{u} = \mathbf{0}, \quad (15)$$

$$\mathbf{Z}_\Omega^T \mathbf{e}_n = \mathbf{0}, \quad n \notin \Omega \quad (16)$$

$$\mathbf{Z}_\Omega^T \mathbf{Z}_\Omega = \mathbf{I}, \quad (17)$$

$$\mathbf{Z}_\Omega \mathbf{Z}_\Omega^T = \mathbf{I} - [\mathbf{u} \ \mathbf{E}_{\bar{\Omega}}] \left( \begin{bmatrix} \mathbf{u}^T \\ \mathbf{E}_{\bar{\Omega}}^T \end{bmatrix} [\mathbf{u} \ \mathbf{E}_{\bar{\Omega}}] \right)^{-1} \begin{bmatrix} \mathbf{u}^T \\ \mathbf{E}_{\bar{\Omega}}^T \end{bmatrix}. \quad (18)$$

- Since  $\mathcal{G}$  is connected, we must have  $M \geq N - 1$ . The nullspace of  $\mathbf{B}$  is one-dimensional and spanned by  $\mathbf{u}$ :  $\mathbf{B} \mathbf{u} = \mathbf{0}$ . The column rank of  $\mathbf{B}$  is  $N - 1$ . The columns of  $\mathbf{Z}$  span the columns of  $\mathbf{B}^T$  and of  $(\mathbf{Q}^{-1/2} \mathbf{B})^T$ .
- Since the “ $\Omega$ -part” of  $\mathcal{G}_\Omega$  is connected, we must have  $M_\Omega \geq N_\Omega - 1$ . Furthermore,  $\mathbf{B}_\Omega$  has column rank  $N_\Omega - 1$ . Its nullspace is spanned by  $\{\mathbf{u}, \mathbf{E}_{\bar{\Omega}}\}$ . The columns of  $\mathbf{Z}_\Omega$  span the columns of  $\mathbf{B}_\Omega^T$  and of  $(\mathbf{Q}_\Omega^{-1/2} \mathbf{B}_\Omega)^T$ .

### C. Least-Squares Estimate of $\{\phi_n\}$ in Case (a)

In case (a), the least-squares estimate of  $\phi$ , given the pre-whitened measurements in (4) obtained from the nominal graph  $\mathcal{G}$ , is

$$\underset{\phi}{\operatorname{argmin}} \|\mathbf{x}' - \mathbf{Q}^{-1/2} \mathbf{B} \phi\|^2. \quad (19)$$

Since the column space of  $(\mathbf{Q}^{-1/2} \mathbf{B})^T$  is spanned by  $\mathbf{Z}$ ,  $\phi$  can be identified up to a vector proportional to  $\mathbf{u}$ . More precisely, (19) has the solutions

$$\hat{\phi} = \mathbf{Z} \hat{\mathbf{s}} + \lambda \mathbf{u}, \quad (20)$$

where

$$\hat{\mathbf{s}} = (\mathbf{Z}^T \mathbf{B}^T \mathbf{Q}^{-1} \mathbf{B} \mathbf{Z})^{-1} \mathbf{Z}^T \mathbf{B}^T \mathbf{Q}^{-1} \mathbf{x}, \quad (21)$$

and  $\lambda$  is an indeterminate scalar.

While  $\hat{\mathbf{s}}$  is uniquely determined,  $\lambda$  is not. Fortunately,  $\lambda$  does not affect beamforming performance (Section III). Hence, we can set  $\lambda = 0$ . This yields the unique solution

$$\hat{\phi} = \mathbf{Z} \hat{\mathbf{s}} = \mathbf{Z} (\mathbf{Z}^T \mathbf{B}^T \mathbf{Q}^{-1} \mathbf{B} \mathbf{Z})^{-1} \mathbf{Z}^T \mathbf{B}^T \mathbf{Q}^{-1} \mathbf{x}. \quad (22)$$

Note, in passing, that among all solutions to (19), (22) is the one with the smallest  $\|\phi\|$ .

A direct calculation yields

$$\begin{aligned} \mathbb{E}\{\hat{\phi}\} &= \mathbb{E}\{\mathbf{Z} (\mathbf{Z}^T \mathbf{B}^T \mathbf{Q}^{-1} \mathbf{B} \mathbf{Z})^{-1} \mathbf{Z}^T \mathbf{B}^T \mathbf{Q}^{-1} (\mathbf{B} \phi + \mathbf{w})\} \\ &= \mathbf{Z} (\mathbf{Z}^T \mathbf{B}^T \mathbf{Q}^{-1} \mathbf{B} \mathbf{Z})^{-1} \mathbf{Z}^T \mathbf{B}^T \mathbf{Q}^{-1} \\ &\quad \cdot \mathbb{E}\left\{ \mathbf{B} \left( \mathbf{Z} \mathbf{Z}^T + \frac{1}{N} \mathbf{u} \mathbf{u}^T \right) \phi + \mathbf{w} \right\} \\ &= \mathbf{Z} \mathbf{Z}^T \phi, \end{aligned} \quad (23)$$

$$\operatorname{Cov}\{\hat{\phi}\} = \mathbf{Z} (\mathbf{Z}^T \mathbf{B}^T \mathbf{Q}^{-1} \mathbf{B} \mathbf{Z})^{-1} \mathbf{Z}^T = \mathbf{Z} (\mathbf{Z}^T \mathbf{L} \mathbf{Z})^{-1} \mathbf{Z}^T. \quad (24)$$

In the last step of (23), we used that  $\mathbf{B} \mathbf{u} = \mathbf{0}$  and that  $\mathbb{E}\{\mathbf{w}\} = \mathbf{0}$ . In (24), we additionally used that  $\operatorname{Cov}\{\mathbf{w}\} = \mathbf{Q}$ . Equation (23) implies that the part of  $\hat{\phi}$  that lies outside the unidentifiable (and uninteresting) subspace spanned by  $\mathbf{u}$  is unbiased. This means that (24) completely quantifies the accuracy of  $\hat{\phi}$ . Note that  $\operatorname{Cov}\{\hat{\phi}\}$  is rank-deficient – a consequence of the non-identifiability of  $\lambda$ .

### D. Monotonicity of $\operatorname{Cov}\{\hat{\phi}\}$ in Case (a)

For fixed  $N$ , by adding more measurements the accuracy of  $\{\hat{\phi}\}$  improves. To see this, suppose the nominal  $\mathbf{B}$  is replaced by

$$\mathbf{B}'' = \begin{bmatrix} \mathbf{B}' \\ \mathbf{B} \end{bmatrix}, \quad (25)$$

for some  $\mathbf{B}'$  that represents the additional measurements. Let  $\mathbf{Q}''$  be the noise covariance of the augmented measurement set, such that  $\mathbf{Q}$  is the lower-right  $N \times N$  submatrix of  $\mathbf{Q}''$ . Explicitly, partition  $\mathbf{Q}''$  according to

$$\mathbf{Q}'' = \begin{bmatrix} \bar{\mathbf{Q}} & \tilde{\mathbf{Q}}^T \\ \tilde{\mathbf{Q}} & \mathbf{Q} \end{bmatrix}. \quad (26)$$

Let

$$\mathbf{L}'' = \mathbf{B}'^T \mathbf{Q}''^{-1} \mathbf{B}', \quad (27)$$

and let  $\mathbf{Z}''$  be the counterpart of  $\mathbf{Z}$  associated with  $\mathbf{L}''$ . By rewriting  $\mathbf{Q}''^{-1}$  using a Schur complement, we obtain (28), shown on top of the next page. Since  $\mathbf{Q} \succcurlyeq \mathbf{Q} - \tilde{\mathbf{Q}}\bar{\mathbf{Q}}^{-1}\tilde{\mathbf{Q}}^T$ , we have using Corollary 7.7.4(a) of [38] that

$$(\mathbf{Q} - \tilde{\mathbf{Q}}\bar{\mathbf{Q}}^{-1}\tilde{\mathbf{Q}}^T)^{-1} - \mathbf{Q}^{-1} \succcurlyeq \mathbf{0}. \quad (29)$$

Therefore, the matrix in the middle of the right hand side of (28) is positive semidefinite, from which it follows that the right hand side of (28) is positive semidefinite (note its Gramian form). We conclude that  $\mathbf{L}'' \succcurlyeq \mathbf{L}$ , wherefrom it follows that  $\mathbf{Z}''^T \mathbf{L}'' \mathbf{Z}'' \succcurlyeq \mathbf{Z}^T \mathbf{L} \mathbf{Z}$ . By applying again Corollary 7.7.4(a) of [38], we find that

$$(\mathbf{Z}''^T \mathbf{L}'' \mathbf{Z}'')^{-1} \succcurlyeq (\mathbf{Z}^T \mathbf{L} \mathbf{Z})^{-1}. \quad (30)$$

The nullspaces of  $\mathbf{L}$  and  $\mathbf{L}''$  are one-dimensional and spanned by  $\mathbf{u}$ . Therefore,  $\mathbf{Z}$  and  $\mathbf{Z}''$  have the same column space. It follows that there exists an  $(N-1) \times (N-1)$  matrix  $\Psi$  such that

$$\mathbf{Z}'' \Psi = \mathbf{Z} \quad (31)$$

$$\Psi^T \Psi = \Psi \Psi^T = \mathbf{I}. \quad (32)$$

Therefore,

$$\begin{aligned} & \mathbf{Z}(\mathbf{Z}^T \mathbf{L} \mathbf{Z})^{-1} \mathbf{Z}^T - \mathbf{Z}''(\mathbf{Z}''^T \mathbf{L}'' \mathbf{Z}'')^{-1} \mathbf{Z}''^T \\ &= \mathbf{Z}'' \Psi (\Psi^T \mathbf{Z}''^T \mathbf{L}'' \mathbf{Z}'' \Psi)^{-1} \Psi^T \mathbf{Z}''^T \\ & \quad - \mathbf{Z}''(\mathbf{Z}''^T \mathbf{L}'' \mathbf{Z}'')^{-1} \mathbf{Z}''^T \\ &= \mathbf{Z}''(\mathbf{Z}''^T \mathbf{L}'' \mathbf{Z}'')^{-1} \mathbf{Z}''^T - \mathbf{Z}''(\mathbf{Z}''^T \mathbf{L}'' \mathbf{Z}'')^{-1} \mathbf{Z}''^T \\ &= \mathbf{Z}'' \left( (\mathbf{Z}''^T \mathbf{L}'' \mathbf{Z}'')^{-1} - (\mathbf{Z}''^T \mathbf{L}'' \mathbf{Z}'')^{-1} \right) \mathbf{Z}''^T \succcurlyeq \mathbf{0}, \end{aligned} \quad (33)$$

where in the last step we used (30). That is, the difference between  $\text{Cov}\{\hat{\phi}\}$  without the additional measurements, and  $\text{Cov}\{\hat{\phi}\}$  with those measurements, is positive semidefinite.

### E. Least-Squares Estimate of $\{\phi_n\}$ in Case (b)

In case (b), the corresponding least-squares problem is

$$\underset{\phi}{\text{argmin}} \|\mathbf{x}'_{\Omega} - \mathbf{Q}_{\Omega}^{-1/2} \mathbf{B}_{\Omega} \phi\|^2. \quad (34)$$

Problem (34) has the solutions

$$\hat{\phi} = \mathbf{Z}_{\Omega} \hat{\mathbf{s}}_{\Omega} + \lambda \mathbf{u} + \sum_{n \notin \Omega} \lambda_n \mathbf{e}_n, \quad (35)$$

where

$$\hat{\mathbf{s}}_{\Omega} = (\mathbf{Z}_{\Omega}^T \mathbf{B}_{\Omega}^T \mathbf{Q}_{\Omega}^{-1} \mathbf{B}_{\Omega} \mathbf{Z}_{\Omega})^{-1} \mathbf{Z}_{\Omega}^T \mathbf{B}_{\Omega}^T \mathbf{Q}_{\Omega}^{-1} \mathbf{x}_{\Omega}, \quad (36)$$

and  $\lambda$  and  $\{\lambda_n\}$  are indeterminate scalars that we will set to zero. The mean and covariance can be found via a similar calculation as in Section II-C, using the above-established facts about  $\mathbf{L}_{\Omega}$ ,  $\mathbf{Z}_{\Omega}$ , and  $\mathbf{B}_{\Omega}$ :

$$\mathbb{E}\{\hat{\phi}\} = \mathbf{Z}_{\Omega} \mathbf{Z}_{\Omega}^T \phi, \quad (37)$$

$$\text{Cov}\{\hat{\phi}\} = \mathbf{Z}_{\Omega} (\mathbf{Z}_{\Omega}^T \mathbf{L}_{\Omega} \mathbf{Z}_{\Omega})^{-1} \mathbf{Z}_{\Omega}^T. \quad (38)$$

Note that  $\text{Var}\{\hat{\phi}_n\}$  for  $n \in \Omega$  is not necessarily larger in case (b) than in case (a), even though in case (a) we have more measurements, because in case (a) there are more identifiable parameters.

## III. BEAMFORMING GAIN ANALYSIS

Next we examine the impact of estimation errors in  $\{\hat{\phi}_n\}$  on joint coherent downlink beamforming performance, when targeting a specific point (focal spot) in space with reciprocity-based beamforming. The beamforming is performed by the antennas in the set  $\Omega$ .

To keep the analysis clean, we restrict the discussion to the beamforming of a monochromatic (sinusoidal) signal with some given carrier frequency. The argument extends directly to any signal whose bandwidth is less than the channel coherence bandwidth (reciprocal excess delay).<sup>2</sup> Also, nothing prevents the application of the analysis to multiple narrowband signals that are adjacent in the frequency domain. Let  $h_n$  be the channel frequency response (complex-baseband channel gain) at the carrier frequency of concern, between the  $n$ th antenna and the focal spot, and let  $a_n$  be the respective beamforming weight applied by the  $n$ th antenna.

Suppose that the above-described estimates  $\{\hat{\phi}_n\}$  are used to pre-compensate  $\{a_n\}$  when performing the beamforming. The effective channel to the focal spot is then

$$g = \sum_{n \in \Omega} h_n a_n e^{j\hat{\phi}_n} e^{-j\phi_n}. \quad (39)$$

The corresponding beamforming (power) gain is  $|g|^2$ . Adding a common constant to all  $\{\hat{\phi}_n\}$  does not affect  $|g|$ , which is why we can safely set  $\lambda = 0$  and  $\lambda_n = 0$  in Section II.

### A. Beamforming for Constructive Interference

If  $\{\phi_n\}$  are perfectly known, then  $|g|$  can be made to scale with  $N$ , by taking the angle of  $a_n$  to align with that of  $h_n^*$ , causing constructive interference at the focal spot. This gives the standard coherent array gain.

If  $\{\phi_n\}$  are only imperfectly known, the array gain deteriorates. In practice, accurate knowledge is not critical. For example, suppose  $|h_n| = 1$  and that  $\{\phi_n\}$  for half of the antennas are perfectly known, but that  $\{\phi_n\}$  for the other antennas are off by  $\delta$  radians. The relative loss in  $|g|^2$  is then  $|1 + 1|^2 / |1 + e^{j\delta}|^2$ . Even if  $\delta = \pi/2$  ( $90^\circ$ ) the loss is only 3 dB. But beyond  $90^\circ$  errors, the array gain quickly evaporates. We omit a detailed analysis and instead focus on the more interesting case of null-steering, next.

<sup>2</sup>Technically, a finite excess-delay assumption is inconsistent with an array aperture that grows to infinity. In practice, signals originating at antennas farther and farther away would be attenuated more and more strongly, eventually contributing negligibly to the channel response.

$$\begin{aligned}
L'' - L &= \mathbf{B}''^T \mathbf{Q}''^{-1} \mathbf{B}'' - \mathbf{B}^T \mathbf{Q}^{-1} \mathbf{B} \\
&= \mathbf{B}''^T \mathbf{Q}''^{-1} \mathbf{B}'' - \mathbf{B}''^T \begin{bmatrix} \mathbf{0} \\ \mathbf{I} \end{bmatrix} \mathbf{Q}^{-1} \begin{bmatrix} \mathbf{0} & \mathbf{I} \end{bmatrix} \mathbf{B}'' \\
&= \mathbf{B}''^T \left( \mathbf{Q}''^{-1} - \begin{bmatrix} \mathbf{0} \\ \mathbf{I} \end{bmatrix} \mathbf{Q}^{-1} \begin{bmatrix} \mathbf{0} & \mathbf{I} \end{bmatrix} \right) \mathbf{B}'' \\
&= \mathbf{B}''^T \left( \begin{bmatrix} \mathbf{I} & -\bar{\mathbf{Q}}^{-1} \tilde{\mathbf{Q}}^T \\ \mathbf{0} & \mathbf{I} \end{bmatrix} \begin{bmatrix} \bar{\mathbf{Q}}^{-1} & \mathbf{0} \\ \mathbf{0} & (\mathbf{Q} - \tilde{\mathbf{Q}} \bar{\mathbf{Q}}^{-1} \tilde{\mathbf{Q}}^T)^{-1} \end{bmatrix} \begin{bmatrix} \mathbf{I} & \mathbf{0} \\ -\tilde{\mathbf{Q}} \bar{\mathbf{Q}}^{-1} & \mathbf{I} \end{bmatrix} - \begin{bmatrix} \mathbf{0} \\ \mathbf{I} \end{bmatrix} \mathbf{Q}^{-1} \begin{bmatrix} \mathbf{0} & \mathbf{I} \end{bmatrix} \right) \mathbf{B}'' \\
&= \mathbf{B}''^T \begin{bmatrix} \mathbf{I} & -\bar{\mathbf{Q}}^{-1} \tilde{\mathbf{Q}}^T \\ \mathbf{0} & \mathbf{I} \end{bmatrix} \begin{bmatrix} \bar{\mathbf{Q}}^{-1} & \mathbf{0} \\ \mathbf{0} & (\mathbf{Q} - \tilde{\mathbf{Q}} \bar{\mathbf{Q}}^{-1} \tilde{\mathbf{Q}}^T)^{-1} - \mathbf{Q}^{-1} \end{bmatrix} \begin{bmatrix} \mathbf{I} & \mathbf{0} \\ -\tilde{\mathbf{Q}} \bar{\mathbf{Q}}^{-1} & \mathbf{I} \end{bmatrix} \mathbf{B}'' \tag{28}
\end{aligned}$$

### B. Beamforming for Destructive Interference

With null-steering,  $\{a_n\}$  are selected such that the signals from different antennas interfere *destructively* at the focal spot:

$$\sum_{n \in \Omega} h_n a_n = 0, \tag{40}$$

attempting to make  $g = 0$ . This is the operational principle of zero-forcing beamforming for multiuser MIMO [39], [40].

To analyze the beamforming gain in the presence of phase estimation errors, consider first case (a). Recall that  $\{\hat{\phi}_n - \phi_n\}$  have nonzero mean because of the non-identifiability of the estimation problem; see (23). For analysis purposes, it will prove useful to introduce the following intermediate quantities:

$$\tilde{\phi}_n = \hat{\phi}_n - \phi_n + \bar{\phi}, \tag{41}$$

where we defined the average of the phase values,

$$\bar{\phi} = \frac{1}{N} \sum_{n=1}^N \phi_n = \frac{\mathbf{u}^T \boldsymbol{\phi}}{N}. \tag{42}$$

One can think of  $\{\tilde{\phi}_n\}$  as the “zero-mean part” of the estimation errors, because  $\mathbb{E}\{\tilde{\phi}_n\} = 0$  for all  $n$ . To see why this is so, let  $\tilde{\boldsymbol{\phi}} = [\tilde{\phi}_1, \dots, \tilde{\phi}_N]^T$  and note that from (13), (23), (41) and (42) we have that

$$\mathbb{E}\{\tilde{\boldsymbol{\phi}}\} = \mathbf{Z} \mathbf{Z}^T \boldsymbol{\phi} - \boldsymbol{\phi} + \frac{\mathbf{u} \mathbf{u}^T}{N} \boldsymbol{\phi} = \mathbf{0}. \tag{43}$$

We now re-express the effective channel in (39) in terms of  $\{\tilde{\phi}_n\}$  and  $\{\bar{\phi}_n\}$ :

$$\begin{aligned}
g &= \sum_{n \in \Omega} h_n a_n e^{j\hat{\phi}_n} e^{-j\phi_n} = e^{-j\bar{\phi}} \sum_{n \in \Omega} h_n a_n e^{j\tilde{\phi}_n} \\
&\approx e^{-j\bar{\phi}} \sum_{n \in \Omega} h_n a_n (1 + j\tilde{\phi}_n) \\
&= e^{-j(\bar{\phi} - \pi/2)} \sum_{n \in \Omega} h_n a_n \tilde{\phi}_n, \tag{44}
\end{aligned}$$

where in the third step we performed a first-order Taylor expansion,  $e^x \approx 1 + x$ . This expansion is justified since  $\{\tilde{\phi}_n\}$  have zero mean, and in the limit of weak measurement noise they would fluctuate only slightly. In the last step of (44) we used (40).

Next, consider case (b). The analysis is analogous to the one for case (a), but with  $\bar{\phi}$  re-defined. Specifically, in contrast to (42), now we set

$$\bar{\phi} = [1 \quad \mathbf{0}^T] \left( \begin{bmatrix} \mathbf{u}^T \\ \mathbf{E}_{\Omega}^T \end{bmatrix} [\mathbf{u} \quad \mathbf{E}_{\Omega}] \right)^{-1} \begin{bmatrix} \mathbf{u}^T \\ \mathbf{E}_{\Omega}^T \end{bmatrix} \boldsymbol{\phi}, \tag{45}$$

and note that for  $n \in \Omega$ , it holds that  $e_n^T [\mathbf{u} \quad \mathbf{E}_{\Omega}] = [1 \quad \mathbf{0}^T]$ ; therefore, for  $n \in \Omega$ , we have

$$e_n^T [\mathbf{u} \quad \mathbf{E}_{\Omega}] \left( \begin{bmatrix} \mathbf{u}^T \\ \mathbf{E}_{\Omega}^T \end{bmatrix} [\mathbf{u} \quad \mathbf{E}_{\Omega}] \right)^{-1} \begin{bmatrix} \mathbf{u}^T \\ \mathbf{E}_{\Omega}^T \end{bmatrix} \boldsymbol{\phi} = \bar{\phi}. \tag{46}$$

Using (18) and (37) we then find that for  $n \in \Omega$ ,

$$\mathbb{E}\{\hat{\phi}_n\} = e_n^T \mathbf{Z}_{\Omega} \mathbf{Z}_{\Omega}^T \boldsymbol{\phi} = \phi_n - \bar{\phi}. \tag{47}$$

Letting, as before,  $\tilde{\phi}_n = \hat{\phi}_n - \phi_n + \bar{\phi}$ , we have that

$$\mathbb{E}\{\tilde{\phi}_n\} = \phi_n - \bar{\phi} - \phi_n + \bar{\phi} = 0 \tag{48}$$

for  $n \in \Omega$ . This means that the formula for the effective channel, (44), applies to case (b), as well.

Consequently, we have for both cases (a) and (b), that

$$g \approx e^{-j(\bar{\phi} - \pi/2)} \cdot \mathbf{v}^T \tilde{\boldsymbol{\phi}}, \tag{49}$$

where  $\mathbf{v}$  is an  $N$ -vector whose components are

$$v_n = \begin{cases} h_n a_n, & n \in \Omega \\ 0, & \text{otherwise.} \end{cases} \tag{50}$$

In either case,  $\tilde{\boldsymbol{\phi}}$  has zero mean, and covariance  $\text{Cov}\{\tilde{\boldsymbol{\phi}}\} = \text{Cov}\{\hat{\boldsymbol{\phi}}\}$ , given by (24) and (38), respectively. It follows that

$$\mathbb{E}\{g\} \approx 0, \tag{51}$$

$$\text{Var}\{g\} \approx \mathbf{v}^T \text{Cov}\{\hat{\boldsymbol{\phi}}\} \mathbf{v}^* = \mathbf{v}^H \text{Cov}\{\hat{\boldsymbol{\phi}}\} \mathbf{v}, \tag{52}$$

with the respective (real-valued) covariance matrices in (24) and (38) inserted for  $\text{Cov}\{\hat{\boldsymbol{\phi}}\}$ .

## IV. BEAMFORMING GAIN COMPARISON

Henceforth, we are only interested in null-steering. The variance of  $g$ ,  $\text{Var}\{g\}$ , quantifies the beamforming accuracy in terms of how much power inadvertently reaches the focal point, for an arbitrary choice of beamforming weights  $\{a_n\}$  satisfying (40). (The smaller the variance, the better the

accuracy.) We will now compare this variance, for given  $\{a_n\}$ , between the following two cases:

- (a) Beamforming is undertaken by the subset  $\Omega$  of the antennas, and  $\{\hat{\phi}_n\}$  are obtained from calibration measurements among *all*  $N$  antennas, that is, from  $\mathcal{G}$ .
- (b) Beamforming is undertaken by the subset  $\Omega$  of the antennas, but  $\{\hat{\phi}_n\}$  are obtained *only* from calibration measurements among antennas that participate in the beamforming, that is, from  $\mathcal{G}_\Omega$ .

First note from (50) that (40) can be equivalently written as  $\sum_n v_n = 0$ ; that is, using vector notation,

$$\mathbf{u}^T \mathbf{v} = 0. \quad (53)$$

Also, note that the constraint that  $v_n = 0$  for  $n \notin \Omega$  in (50) can be expressed as

$$\mathbf{e}_n^T \mathbf{v} = 0, \quad n \notin \Omega. \quad (54)$$

Taken together, this means that the set of possible beamforming weights  $\{a_n\}$  is defined by the set of  $N$ -vectors  $\mathbf{v}$  that satisfy (53) and (54). Since the columns of  $\mathbf{Z}_\Omega$  span the orthogonal complement of the space spanned by  $\{\mathbf{u}, \mathbf{E}_{\bar{\Omega}}\}$ , we know that for an arbitrary vector  $\mathbf{v}$  that satisfies (53)–(54), there exists a unique  $(N_\Omega - 1)$ -vector  $\mathbf{p}$  such that

$$\mathbf{v} = \mathbf{Z}_\Omega \mathbf{p}. \quad (55)$$

In case (a), the variance (52) is given by the quadratic form

$$\begin{aligned} V_a &= \mathbf{v}^H \mathbf{Z} (\mathbf{Z}^T \mathbf{L} \mathbf{Z})^{-1} \mathbf{Z}^T \mathbf{v} \\ &= \mathbf{p}^H \mathbf{Z}_\Omega^T \mathbf{Z} (\mathbf{Z}^T \mathbf{L} \mathbf{Z})^{-1} \mathbf{Z}^T \mathbf{Z}_\Omega \mathbf{p} \\ &= \mathbf{p}^H \mathbf{K}_a \mathbf{p}, \end{aligned} \quad (56)$$

where we defined the kernel,

$$\mathbf{K}_a = \mathbf{Z}_\Omega^T \mathbf{Z} (\mathbf{Z}^T \mathbf{L} \mathbf{Z})^{-1} \mathbf{Z}^T \mathbf{Z}_\Omega. \quad (57)$$

In case (b), the variance is

$$\begin{aligned} V_b &= \mathbf{v}^H \mathbf{Z}_\Omega (\mathbf{Z}_\Omega^T \mathbf{L}_\Omega \mathbf{Z}_\Omega)^{-1} \mathbf{Z}_\Omega^T \mathbf{v} \\ &= \mathbf{p}^H \mathbf{Z}_\Omega^T \mathbf{Z}_\Omega (\mathbf{Z}_\Omega^T \mathbf{L}_\Omega \mathbf{Z}_\Omega)^{-1} \mathbf{Z}_\Omega^T \mathbf{Z}_\Omega \mathbf{p} \\ &= \mathbf{p}^H (\mathbf{Z}_\Omega^T \mathbf{L}_\Omega \mathbf{Z}_\Omega)^{-1} \mathbf{p} \\ &= \mathbf{p}^H \mathbf{K}_b \mathbf{p}, \end{aligned} \quad (58)$$

where

$$\mathbf{K}_b = (\mathbf{Z}_\Omega^T \mathbf{L}_\Omega \mathbf{Z}_\Omega)^{-1}. \quad (59)$$

We are now going to establish that  $V_b \geq V_a$  for any  $\mathbf{p}$ , from which it then follows that  $V_b \geq V_a$  for any  $\mathbf{v}$  that satisfies (53)–(54), and therefore for any  $\{a_n\}$  that satisfy (40). Clearly, this is the case if we can demonstrate that  $\mathbf{K}_b \succcurlyeq \mathbf{K}_a$ . From Corollary 7.7.4(a) of [38], we know that  $\mathbf{K}_b \succcurlyeq \mathbf{K}_a$  if and only if  $\mathbf{K}_a^{-1} \succcurlyeq \mathbf{K}_b^{-1}$ . Therefore, the sought-after result follows if we can show that  $\mathbf{K}_a^{-1} - \mathbf{K}_b^{-1} \succcurlyeq \mathbf{0}$ .

The complication in the analysis lies in the rank-deficiency of  $\mathbf{L}$  and  $\mathbf{L}_\Omega$ . To tackle this, note that  $\mathbf{Z}$  and  $[\mathbf{Z}_\Omega \ \mathbf{E}_{\bar{\Omega}}]$  have the same column space; hence, there exists an  $(N - 1) \times (N - 1)$  matrix  $\Psi$  such that

$$\mathbf{Z}\Psi = [\mathbf{Z}_\Omega \ \mathbf{E}_{\bar{\Omega}}], \quad (60)$$

$$\Psi^T \Psi = \Psi \Psi^T = \mathbf{I}. \quad (61)$$

By multiplying (60) from the left by  $\mathbf{Z}_\Omega^T$  and from the right by  $\Psi^T$ , we find that

$$\mathbf{Z}_\Omega^T \mathbf{Z} = [\mathbf{I} \ \mathbf{0}] \Psi^T. \quad (62)$$

It follows that

$$\begin{aligned} \mathbf{K}_a &= \mathbf{Z}_\Omega^T \mathbf{Z} (\mathbf{Z}^T \mathbf{L} \mathbf{Z})^{-1} \mathbf{Z}^T \mathbf{Z}_\Omega \\ &= [\mathbf{I} \ \mathbf{0}] \Psi^T (\mathbf{Z}^T \mathbf{L} \mathbf{Z})^{-1} \Psi \begin{bmatrix} \mathbf{I} \\ \mathbf{0} \end{bmatrix} \\ &= [\mathbf{I} \ \mathbf{0}] \left( \begin{bmatrix} \mathbf{Z}_\Omega^T \\ \mathbf{E}_{\bar{\Omega}}^T \end{bmatrix} \mathbf{L} [\mathbf{Z}_\Omega \ \mathbf{E}_{\bar{\Omega}}] \right)^{-1} \begin{bmatrix} \mathbf{I} \\ \mathbf{0} \end{bmatrix} \\ &= \left( \mathbf{Z}_\Omega^T \mathbf{L} \mathbf{Z}_\Omega - \mathbf{Z}_\Omega^T \mathbf{L} \mathbf{E}_{\bar{\Omega}} (\mathbf{E}_{\bar{\Omega}}^T \mathbf{L} \mathbf{E}_{\bar{\Omega}})^{-1} \mathbf{E}_{\bar{\Omega}}^T \mathbf{L} \mathbf{Z}_\Omega \right)^{-1}, \end{aligned} \quad (63)$$

where in the last step, we used the block matrix inversion lemma.<sup>3</sup>

We have already assumed that the edges of the graph are ordered such that

$$\mathbf{B} = \begin{bmatrix} \mathbf{B}''' \\ \mathbf{B}_\Omega \end{bmatrix}, \quad (64)$$

for some  $\mathbf{B}'''$ . Define

$$\begin{aligned} \Delta &= \mathbf{L} - \mathbf{L}_\Omega = \mathbf{B}^T \mathbf{Q}^{-1} \mathbf{B} - \mathbf{B}_\Omega^T \mathbf{Q}_\Omega^{-1} \mathbf{B}_\Omega \\ &= \mathbf{B}^T \mathbf{Q}^{-1} \mathbf{B} - \mathbf{B}^T \begin{bmatrix} \mathbf{0} \\ \mathbf{I} \end{bmatrix} \mathbf{Q}_\Omega^{-1} \begin{bmatrix} \mathbf{0} & \mathbf{I} \end{bmatrix} \mathbf{B} \\ &= \mathbf{B}^T \left( \mathbf{Q}^{-1} - \begin{bmatrix} \mathbf{0} \\ \mathbf{I} \end{bmatrix} \mathbf{Q}_\Omega^{-1} \begin{bmatrix} \mathbf{0} & \mathbf{I} \end{bmatrix} \right) \mathbf{B}. \end{aligned} \quad (65)$$

By recalling that  $\mathbf{Q}_\Omega$  is the lower-right  $N_\Omega \times N_\Omega$  submatrix of  $\mathbf{Q}$ , rewriting  $\mathbf{Q}^{-1}$  using a Schur complement, and performing a calculation similar to that in (28), we conclude that  $\Delta \succcurlyeq \mathbf{0}$ . Also, because of (10),

$$\mathbf{L}_\Omega \mathbf{E}_{\bar{\Omega}} = \mathbf{0}. \quad (66)$$

Using (59) and (63), the difference between the inverse kernels can then be written,

$$\begin{aligned} \mathbf{K}_a^{-1} - \mathbf{K}_b^{-1} &= \mathbf{Z}_\Omega^T \mathbf{L} \mathbf{Z}_\Omega - \mathbf{Z}_\Omega^T \mathbf{L} \mathbf{E}_{\bar{\Omega}} (\mathbf{E}_{\bar{\Omega}}^T \mathbf{L} \mathbf{E}_{\bar{\Omega}})^{-1} \mathbf{E}_{\bar{\Omega}}^T \mathbf{L} \mathbf{Z}_\Omega \\ &\quad - \mathbf{Z}_\Omega^T \mathbf{L}_\Omega \mathbf{Z}_\Omega \\ &= \mathbf{Z}_\Omega^T \left( \mathbf{L} - \mathbf{L}_\Omega - \mathbf{L} \mathbf{E}_{\bar{\Omega}} (\mathbf{E}_{\bar{\Omega}}^T \mathbf{L} \mathbf{E}_{\bar{\Omega}})^{-1} \mathbf{E}_{\bar{\Omega}}^T \mathbf{L} \right) \mathbf{Z}_\Omega \\ &= \mathbf{Z}_\Omega^T \left( \Delta - (\mathbf{L}_\Omega + \Delta) \mathbf{E}_{\bar{\Omega}} (\mathbf{E}_{\bar{\Omega}}^T (\mathbf{L}_\Omega + \Delta) \mathbf{E}_{\bar{\Omega}})^{-1} \right. \\ &\quad \left. \cdot \mathbf{E}_{\bar{\Omega}}^T (\mathbf{L}_\Omega + \Delta) \right) \mathbf{Z}_\Omega \\ &= \mathbf{Z}_\Omega^T \left( \Delta - \Delta \mathbf{E}_{\bar{\Omega}} (\mathbf{E}_{\bar{\Omega}}^T \Delta \mathbf{E}_{\bar{\Omega}})^{-1} \mathbf{E}_{\bar{\Omega}}^T \Delta \right) \mathbf{Z}_\Omega \\ &= \mathbf{Z}_\Omega^T \Delta^{1/2} \left( \mathbf{I} - \Delta^{1/2} \mathbf{E}_{\bar{\Omega}} (\mathbf{E}_{\bar{\Omega}}^T \Delta \mathbf{E}_{\bar{\Omega}})^{-1} \mathbf{E}_{\bar{\Omega}}^T \Delta^{1/2} \right) \\ &\quad \cdot \Delta^{1/2} \mathbf{Z}_\Omega. \end{aligned} \quad (67)$$

<sup>3</sup>Whenever the inverses exist [38, Sec. 0.7.3],

$$\begin{bmatrix} \mathbf{A} & \mathbf{B} \\ \mathbf{C} & \mathbf{D} \end{bmatrix}^{-1} = \begin{bmatrix} (\mathbf{A} - \mathbf{B} \mathbf{D}^{-1} \mathbf{C})^{-1} & \mathbf{A}^{-1} \mathbf{B} (\mathbf{C} \mathbf{A}^{-1} \mathbf{B} - \mathbf{D})^{-1} \\ (\mathbf{C} \mathbf{A}^{-1} \mathbf{B} - \mathbf{D})^{-1} \mathbf{C} \mathbf{A}^{-1} & (\mathbf{D} - \mathbf{C} \mathbf{A}^{-1} \mathbf{B})^{-1} \end{bmatrix}.$$

The matrix inside the parenthesis after the last equality in (67) is the orthogonal projection onto the orthogonal complement of the column space of  $\Delta^{1/2} \mathbf{E}_{\bar{\Omega}}$ . Therefore, (67) is positive semidefinite, and the desired result follows: the beamforming accuracy in case (a) is always better than, or equal to, that in case (b).

As a final remark, we comment on the implications of monotonicity (Section II-D) on the beamforming gain, when adding more measurements. Consider case (a). Let  $V_a$  be the nominal variance, and  $V_a''$  be the variance after the addition of supplementary measurements. From (33) and (56) it is then immediate that  $V_a'' \leq V_a$ , for any permissible  $\{a_n\}$ . This effect must not, of course, be conflated with the conclusion from the comparison between cases (a) and (b) derived above.

## V. EXAMPLES

The estimation errors in  $\{\hat{\phi}_n\}$  can grow fast when scaling up the network. Yet, the beamforming accuracy, for any subset  $\Omega$ , is always better when all measurements are used. This is best illustrated through the study of some special cases.

In all examples, we assume that the measurement noises are uncorrelated, and set the noise variance to one:  $\mathbf{Q} = \mathbf{I}$ . (In the numerical illustrations, we scale  $\mathbf{Q}$ .) In this case,  $\mathbf{L}$  is the standard Laplacian. When reading the examples, it is useful to keep in mind its equivalent definition:  $\mathbf{L} = \mathbf{D} - \mathbf{A}$ , where  $\mathbf{A}$  is the graph adjacency matrix ( $[\mathbf{A}]_{nn'} = 1$  if  $n$  and  $n'$  are connected, and zero otherwise) and  $\mathbf{D}$  is a diagonal matrix with  $\mathbf{A}\mathbf{u}$  on its diagonal.

### A. Linear (Radio Stripe) Topology

First we consider the line (radio stripe) topology in Figure 1, where measurements are only conducted between neighboring antennas. The Laplacian is immediate from its definition:

$$\mathbf{L} = \begin{bmatrix} 1 & -1 & 0 & \cdots & \cdots & \cdots & \cdots & 0 \\ -1 & 2 & -1 & 0 & & & & \vdots \\ 0 & -1 & 2 & -1 & \ddots & & & \vdots \\ \vdots & 0 & \ddots & \ddots & \ddots & \ddots & & \vdots \\ \vdots & & \ddots & \ddots & \ddots & \ddots & 0 & \vdots \\ \vdots & & & \ddots & -1 & 2 & -1 & 0 \\ \vdots & & & & 0 & -1 & 2 & -1 \\ 0 & \cdots & \cdots & \cdots & \cdots & 0 & -1 & 1 \end{bmatrix}. \quad (68)$$

Let

$$\mathbf{y}_n = \begin{bmatrix} \cos\left(\frac{1}{2} \frac{(n-1)\pi}{N}\right) \\ \cos\left(\frac{3}{2} \frac{(n-1)\pi}{N}\right) \\ \vdots \\ \cos\left(\frac{2N-3}{2} \frac{(n-1)\pi}{N}\right) \\ \cos\left(\frac{2N-1}{2} \frac{(n-1)\pi}{N}\right) \end{bmatrix}, \quad (69)$$

for  $n = 1, \dots, N$ . A direct but tedious calculation, or the use of results from [41], shows that  $\{\mathbf{y}_n\}$  are mutually orthogonal and that they are eigenvectors of  $\mathbf{L}$ :

$$\mathbf{L}\mathbf{y}_1 = \mathbf{0} \quad (70)$$

$$\mathbf{L}\mathbf{y}_n = [\mathbf{A}]_{(n-1)(n-1)} \mathbf{y}_n, \quad n = 2, \dots, N, \quad (71)$$

$$\mathbf{y}_n^T \mathbf{y}_{n'} = 0, \quad n \neq n', \quad (72)$$

where the corresponding eigenvalues are

$$[\mathbf{A}]_{(n-1)(n-1)} = 4 \sin^2\left(\frac{(n-1)\pi}{2N}\right). \quad (73)$$

Note that the first eigenvalue is zero; actually,  $\mathbf{y}_1 = \mathbf{u}$ . Taken together, this means that  $\mathbf{Z}$  can be written as  $\mathbf{Z} = [\mathbf{z}_2 \cdots \mathbf{z}_N]$  where

$$\mathbf{z}_n = \frac{\mathbf{y}_n}{\|\mathbf{y}_n\|}. \quad (74)$$

In particular, (14) holds.

It follows that,

$$\begin{aligned} \text{Cov}\{\hat{\phi}\} &= \mathbf{Z}(\mathbf{Z}^T \mathbf{L} \mathbf{Z})^{-1} \mathbf{Z}^T \\ &= \sum_{n=2}^N \frac{\mathbf{z}_n \mathbf{z}_n^T}{[\mathbf{A}]_{(n-1)(n-1)}} = \frac{1}{4} \sum_{n=2}^N \frac{\mathbf{y}_n \mathbf{y}_n^T}{\sin^2\left(\frac{(n-1)\pi}{2N}\right) \|\mathbf{y}_n\|^2}. \end{aligned} \quad (75)$$

Now use (69) to write the  $n$ th diagonal element of  $\text{Cov}\{\hat{\phi}\}$  as

$$\text{Var}\{\hat{\phi}_n\} = \frac{1}{4} \sum_{n'=2}^N \frac{\cos^2\left((2n-1)\frac{(n'-1)\pi}{2N}\right)}{\sin^2\left(\frac{(n'-1)\pi}{2N}\right) \|\mathbf{y}_{n'}\|^2}. \quad (76)$$

The right hand side of (76) can be lower-bounded by retaining only the first two terms, for which  $n' = 2$  and  $n' = 3$ . (Keeping only the first term turns out to be insufficient.) The sum of the numerators corresponding to  $n' = 2$  and  $n' = 3$  is lower-bounded, uniformly over  $n$ , as follows:

$$\begin{aligned} &\cos^2\left((2n-1)\frac{\pi}{2N}\right) + \cos^2\left((2n-1)\frac{\pi}{N}\right) \\ &= \frac{1}{2} \left[ 1 + \cos\left((2n-1)\frac{\pi}{N}\right) + 2 \cos^2\left((2n-1)\frac{\pi}{N}\right) \right] \\ &= \frac{1}{2} \left[ 1 + \frac{1}{2} \cos\left((2n-1)\frac{\pi}{N}\right) \right]^2 + \frac{7}{8} \cos^2\left((2n-1)\frac{\pi}{N}\right) \\ &\geq \frac{1}{8}. \end{aligned} \quad (77)$$

From (69) it is immediate that

$$\|\mathbf{y}_n\|^2 \leq N, \quad n = 1, \dots, N. \quad (78)$$

Since  $\sin(x) \leq x$  for  $x \geq 0$ , the denominator of the terms inside the sum of (76) for  $n' = 2$  and  $n' = 3$  is upper-bounded by,

$$\sin^2\left(\frac{(n'-1)\pi}{2N}\right) \|\mathbf{y}_{n'}\|^2 \leq \left(\frac{\pi}{N}\right)^2 N = \frac{\pi^2}{N}. \quad (79)$$

Putting these bounds together we find that uniformly over  $n$ ,

$$\text{Var}\{\hat{\phi}_n\} \geq \frac{N}{32\pi^2}. \quad (80)$$

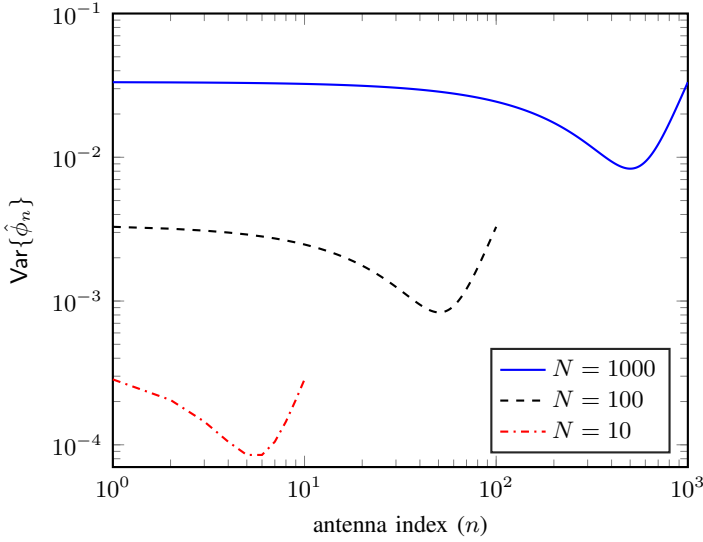


Fig. 3.  $\text{Var}\{\hat{\phi}_n\}$  as function of antenna index  $n$ , for different total numbers of antennas,  $N$ , for the line (radio stripe) topology in Figure 1, for  $\mathbf{Q} = 10^{-4} \cdot \mathbf{I}$ . Note the logarithmic scale; the minimum occurs when  $n = N/2$ .

This shows that the smallest value among  $\text{Var}\{\hat{\phi}_n\} \rightarrow \infty$  as  $N \rightarrow \infty$  (rather quickly). Despite this, we know, from the analysis in Section IV, that the beamforming accuracy for any fixed subset  $\Omega$  cannot decrease when including more antennas in the calibration process. In this particular example with a line topology, it turns out that  $\mathbf{K}_a = \mathbf{K}_b$  (see below), but we will see an example later (Section V-C) where  $\mathbf{K}_b$  is strictly larger than  $\mathbf{K}_a$ .

To see why  $\mathbf{K}_a = \mathbf{K}_b$  in the present example, consider first the case that  $\Omega = \{1, \dots, N_\Omega\}$ , and look at the penultimate line of (67). Let  $\Psi = \Delta - \Delta \mathbf{E}_{\bar{\Omega}} (\mathbf{E}_{\bar{\Omega}}^T \Delta \mathbf{E}_{\bar{\Omega}})^{-1} \mathbf{E}_{\bar{\Omega}}^T \Delta$  and note that  $\Psi \mathbf{E}_{\bar{\Omega}} = \mathbf{0}$ ; likewise,  $\Psi \mathbf{u} = \mathbf{0}$ . Also note that  $\Delta$  has zeros in its  $(N_\Omega - 1) \times (N_\Omega - 1)$  upper-left corner; so has  $\Psi$ . Since  $\mathbf{u}$  is linearly independent of the columns of  $\mathbf{E}_{\bar{\Omega}}$ , the only possibility is  $\Psi = \mathbf{0}$ , which, by (67), implies  $\mathbf{K}_a = \mathbf{K}_b$ . The case when  $\Omega$  consists of a different set of consecutive indices can be handled similarly.

Figure 3 shows  $\text{Var}\{\hat{\phi}_n\}$  as function of  $n$ , for some different values of  $N$ . The largest variances occur at the ends of the stripe. When  $N \rightarrow \infty$ , the smallest among  $\{\text{Var}\{\hat{\phi}_n\}\}$  (which, as seen in the figure, is in the middle of the stripe) – and therefore all of them – grow without bound.

We remind the reader about the point made earlier regarding arithmetic mod  $2\pi$ . Also, we stress that the inequality (80) is not tight at all; its only purpose is to show the unboundedness.

### B. Ring Topology

A variation on the previous example is a ring topology, obtained from the line topology by connecting nodes 1 and  $N$  (Figure 4). The Laplacian becomes a circulant matrix, which can be diagonalized using the discrete Fourier transform [42]. Because of the symmetry, the eigenvalues of  $\mathbf{L}$  appear in pairs and the eigenvectors appear in complex-conjugated pairs, such

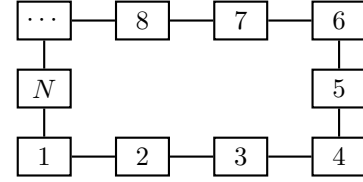


Fig. 4. Ring topology, where every antenna performs measurements on its two neighbors.

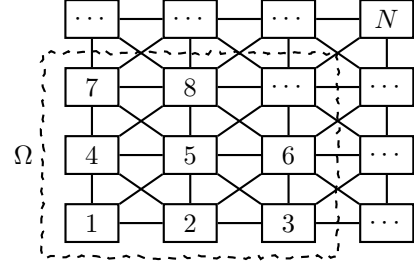


Fig. 5. Large-intelligent-surface topology, where each antenna performs measurements on its north-south, east-west, southeast-northwest and southwest-northeast closest neighbors.

that appropriate linear combinations thereof yield real-valued eigenvectors. Among these eigenvectors, one is

$$\mathbf{z} = \frac{1}{\sqrt{N}} \begin{bmatrix} 1 \\ \cos(2\pi/N) \\ \cos(2 \cdot 2\pi/N) \\ \vdots \\ \cos((N-1)2\pi/N) \end{bmatrix}, \quad (81)$$

which has unit norm,  $\|\mathbf{z}\| = 1$ , and corresponding eigenvalue  $4 \sin^2(\pi/N)$ . (One can alternatively find this eigenvector from results in [41].)

In this example all nodes are statistically identical and a calculation somewhat similar to, but simpler than, the one in Section V-A (we leave the details to the reader) shows that for any  $n$ ,

$$\text{Var}\{\hat{\phi}_n\} \geq \frac{1/N}{4 \sin^2(\pi/N)} \geq \frac{1/N}{4\pi^2/N^2} = \frac{N}{4\pi^2}. \quad (82)$$

Thus as  $N \rightarrow \infty$  the ring exhibits the same behavior as the line topology: the variances grow without bound.

### C. Large-Intelligent-Surface Topology

In the next example we consider a large intelligent surface,<sup>4</sup> envisioned by many as a main physical-layer solution for 6G [5], [44]. The idea is to cover a large surface (for example, a wall or ceiling of a building) by antennas that may be, for aesthetic reasons, physically integrated into the surface itself.

We assume, for the example, that each antenna can perform calibration measurements on its eight closest neighbors (except for the antennas on the border), as shown in Figure 5. The

<sup>4</sup>A large intelligent surface is not to be confused with a *reflecting* intelligent surface (RIS), also known as an intelligent reflecting surface (IRS). The use of a RIS (IRS) entails its own calibration challenges [43], but they are of a totally different kind and unrelated to the material presented herein.

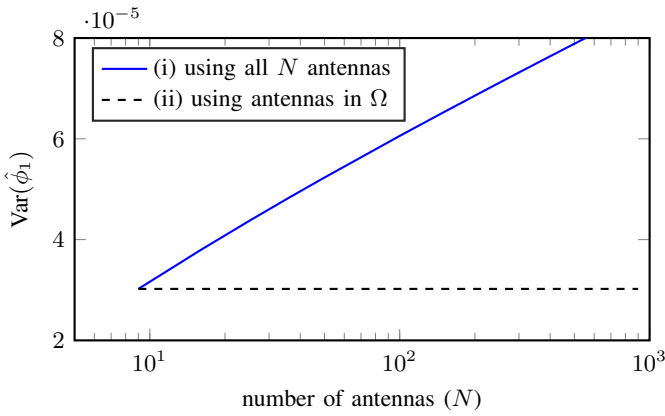


Fig. 6. For the topology in Figure 5, and  $\mathbf{Q} = 10^{-4} \cdot \mathbf{I}$ : (i)  $\text{Var}\{\hat{\phi}_1\}$  when using all available calibration measurements; (ii)  $\text{Var}\{\hat{\phi}_1\}$  when using only the calibration measurements among antennas in  $\Omega$ , consisting of the nine antennas in the  $3 \times 3$  lower left corner of the surface.

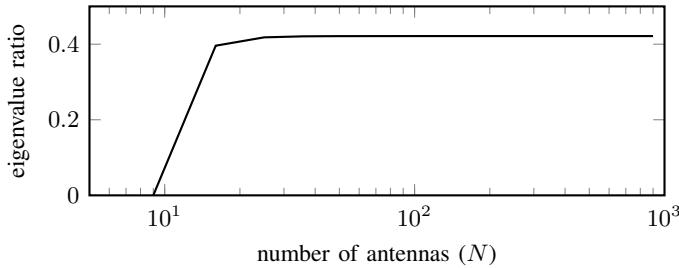


Fig. 7. For the topology in Figure 5: the largest eigenvalue of  $\mathbf{K}_b - \mathbf{K}_a$  relative to the largest eigenvalue of  $\mathbf{K}_b$ .

Laplacian is easily written down but analysis in closed form, beyond the general formulas already obtained, is cumbersome.

Figure 6 shows the following:

- (i) the estimation error variance for the antenna in the lower-left corner (number 1 in Figure 5),  $\text{Var}\{\hat{\phi}_1\}$ , for case (a), when using all  $M$  calibration measurements, and
- (ii)  $\text{Var}\{\hat{\phi}_1\}$  for case (b) when using only the  $M_\Omega$  calibration measurements among antennas in a subset  $\Omega$ , consisting of the nine antennas in the  $3 \times 3$  lower left corner of the surface.

We make the following observations:

- $\text{Var}\{\hat{\phi}_1\}$  in case (a) increases when using more antennas, though not as fast as for the line topology (cf. (80)). We conjecture that the variance is unbounded when  $N \rightarrow \infty$ .
- $\text{Var}\{\hat{\phi}_1\}$  in case (b) is, of course, independent of  $N$ .

Next, Figure 7 shows the largest possible improvement in beamforming accuracy when using all antennas for calibration, compared to when using only the antennas in  $\Omega$ , quantified via the largest eigenvalue of  $\mathbf{K}_b - \mathbf{K}_a$  relative to the largest eigenvalue of  $\mathbf{K}_b$ . This is the largest value that  $V_b - V_a$  can attain relative to the largest possible value that  $V_b$  can attain, for any unit-norm  $\mathbf{v}$ . (Note that  $\|\mathbf{v}\|^2 = \mathbf{v}^H \mathbf{v} = \mathbf{p}^H \mathbf{Z}_\Omega^T \mathbf{Z}_\Omega \mathbf{p} = \mathbf{p}^H \mathbf{p} = \|\mathbf{p}\|^2$ .) A significant improvement in performance when beamforming from antennas in  $\Omega$  can be achieved by using calibration measurements from antennas outside of  $\Omega$ . But the gain levels off

quickly. Beyond  $N = 16$  the curve is almost flat so there is no point in practice in going beyond the  $4 \times 4$  lower-left corner.

#### D. Complete Graph Topology

We end with an exposition of the situation when all  $N$  antennas measure on all others. In this case,  $\mathcal{G}$  is a complete graph with  $M = N(N-1)/2$  edges. The Laplacian is

$$\mathbf{L} = N\mathbf{I} - \mathbf{u}\mathbf{u}^T. \quad (83)$$

Recalling that  $\mathbf{u}^T \mathbf{Z} = \mathbf{0}$ , we find that

$$\text{Cov}\{\hat{\phi}\} = \mathbf{Z}(\mathbf{Z}^T \mathbf{L} \mathbf{Z})^{-1} \mathbf{Z}^T = \frac{1}{N} \mathbf{Z} \mathbf{Z}^T. \quad (84)$$

The variance of  $\hat{\phi}_n$ , for an arbitrary  $n$ , follows as,

$$\begin{aligned} \text{Var}\{\hat{\phi}_n\} &= \mathbf{e}_n^T \text{Cov}\{\hat{\phi}\} \mathbf{e}_n = \frac{1}{N} \mathbf{e}_n^T \mathbf{Z} \mathbf{Z}^T \mathbf{e}_n \\ &= \frac{1}{N} \mathbf{e}_n^T \left( \mathbf{I} - \frac{1}{N} \mathbf{u}\mathbf{u}^T \right) \mathbf{e}_n \\ &= \frac{1}{N} \left( 1 - \frac{1}{N} \right) = \frac{1}{N} - \frac{1}{N^2}. \end{aligned} \quad (85)$$

When adding more and more antennas, this variance goes to zero:  $\text{Var}\{\hat{\phi}_n\} \rightarrow 0$  as  $N \rightarrow \infty$ , uniformly over  $n$ . This is a consequence of the dense topology, and the conclusion is the opposite of that for the other topologies discussed above. In the present example, the number of unknowns is proportional to  $N$ , but the number of measurements is proportional to  $N^2$ , making the problem more and more well-conditioned as  $N$  increases.

## VI. MASSIVE SYNCHRONY

Returning to question Q3 asked in Section I-D, what topologies enable massive synchrony in the sense that  $\{\text{Var}\{\hat{\phi}_n\}\}$  remain bounded, or even vanish, when  $N \rightarrow \infty$ ? For the complete graph (Section V-D), all variances tend to zero. But for the line topology, in contrast (Section V-A) all variances tend to infinity. It appears plausible that the complete graph could be “thinned out” quite substantially before encountering this phenomenon, but it is unclear exactly how much.

One observation is that the average variance can be written in terms of the Laplacian eigenvalues:

$$\begin{aligned} \frac{1}{N} \sum_{n=1}^N \text{Var}\{\hat{\phi}_n\} &= \frac{1}{N} \text{Tr}\{\text{Cov}\{\hat{\phi}\}\} = \frac{1}{N} \text{Tr}\{\mathbf{Z} \mathbf{\Lambda}^{-1} \mathbf{Z}^T\} \\ &= \frac{1}{N} \text{Tr}\{\mathbf{\Lambda}^{-1} \mathbf{Z}^T \mathbf{Z}\} = \frac{1}{N} \text{Tr}\{\mathbf{\Lambda}^{-1}\} \\ &= \frac{1}{N} \sum_{n=1}^{N-1} \frac{1}{[\mathbf{\Lambda}]_{nn}}. \end{aligned} \quad (86)$$

For a tree topology, and for uncorrelated, homoskedastic noise ( $\mathbf{Q} = \mathbf{I}$ ) one can use [45, Theorem 4.3] (see also [46]) to write the right hand side of (86) as a constant times the average distance between pairs of nodes in  $\mathcal{G}$ . For an arbitrary topology, monotonicity (Section II-D) then gives an upper bound on the average variance in terms of the average distance of a spanning tree.

Whether stronger results can be established remains open. These questions might have limited (at best) impact on the operation of distributed antenna systems in practice, but come across as interesting basic research problems.

## VII. CONCLUDING REMARKS

For R-calibration, it is enough to compute a single set of calibration coefficients for the entire network, based on appropriate bidirectional measurements between service antennas, and then use these coefficients for all beamforming activities in the network. This is so despite the fact that the phase estimation errors grow, in some cases without bound, the more antennas are involved in the calibration process. An important consequence is that there is no need to compute calibration coefficients associated with specific “local areas” or specific users. In fact, irrespective of the network size, solving a single global calibration problem, and using the so-obtained phase corrections everywhere in the network, is optimal.

Extensions of the analyses may be possible. For example, one could potentially work directly on  $\{T_n, R_n\}$  to circumvent the assumption on “small” errors induced by the mod  $2\pi$  arithmetic, although this appears very difficult due to the nonlinear nature of the ensuing estimation problem. Also, a complete characterization of topologies for which  $\{\text{Var}\{\hat{\phi}_n\}\}$  are bounded, or vanish, with increasing  $N$ , is an open problem.

The beamforming gain analysis herein applies to reciprocity-based beamforming. Corresponding analyses for other applications, such as sensing and positioning, and for F-calibration, could be of interest too. An additional possible topic for future work is to consider the overhead incurred by calibration measurements, and its effect on the resulting spectral efficiency when the antennas are used for multiuser beamforming.

## ACKNOWLEDGMENT

The author thanks the colleagues in the REINDEER project for extensive discussions on antenna calibration, and Prof. Liesbet Van der Perre for her useful comments on an early draft of the manuscript.

## REFERENCES

- [1] D. Wang, J. Wang, X. You, Y. Wang, M. Chen, and X. Hou, “Spectral efficiency of distributed MIMO systems,” *IEEE Journal on Selected Areas in Communications*, vol. 31, no. 10, pp. 2112–2127, 2013.
- [2] S. Venkatesan, A. Lozano, and R. Valenzuela, “Network MIMO: Overcoming intercell interference in indoor wireless systems,” in *Proc. IEEE Asilomar Conf. Signals, Systems, and Computers*, 2007.
- [3] Ö. T. Demir, E. Björnson, and L. Sanguinetti, “Foundations of user-centric cell-free massive MIMO,” *Foundations and Trends® in Signal Processing*, vol. 14, no. 3-4, pp. 162–472, 2021.
- [4] H. Q. Ngo, A. Ashikhmin, H. Yang, E. G. Larsson, and T. L. Marzetta, “Cell-free massive MIMO versus small cells,” *IEEE Transactions on Wireless Communications*, vol. 16, no. 3, pp. 1834–1850, 2017.
- [5] L. Van der Perre, E. G. Larsson, F. Tufvesson, L. De Strycker, E. Björnson, and O. Edfors, “RadioWeaves for efficient connectivity: analysis and impact of constraints in actual deployments,” in *Asilomar Conference on Signals, Systems, and Computers*, 2019.
- [6] G. Interdonato, E. Björnson, H. Q. Ngo, P. Frenger, and E. G. Larsson, “Ubiquitous cell-free massive MIMO communications,” *EURASIP Journal on Wireless Communications and Networking*, 2019.
- [7] E. G. Larsson and J. Vieira, “Phase calibration of distributed antenna arrays,” *IEEE Communications Letters*, 2023.
- [8] C. Shepard, H. Yu, N. Anand, E. Li, T. Marzetta, R. Yang, and L. Zhong, “Argos: Practical many-antenna base stations,” in *International Conference on Mobile Computing and Networking*, 2012.
- [9] A. Bourdoux, B. Come, and N. Khaled, “Non-reciprocal transceivers in OFDM/SDMA systems: Impact and mitigation,” in *IEEE Radio and Wireless Conference*, 2003, pp. 183–186.
- [10] A. Benzin and G. Caire, “Internal self-calibration methods for large scale array transceiver software-defined radios,” in *International ITG Workshop on Smart Antennas (WSA)*, 2017.
- [11] F. Kaltenberger, J. Haiyong, M. Guillaud, and R. Knopp, “Relative channel reciprocity calibration in MIMO/TDD systems,” in *Proc. Future Network and Mobile Summit*, Florence, Italy, June 2010.
- [12] J. Vieira, F. Rusek, O. Edfors, S. Malkowsky, L. Liu, and F. Tufvesson, “Reciprocity calibration for massive MIMO: Proposal, modeling, and validation,” *IEEE Transactions on Wireless Communications*, vol. 16, no. 5, pp. 3042–3056, 2017.
- [13] P. Zetterberg, “Experimental investigation of TDD reciprocity-based zero-forcing transmit precoding,” *EURASIP J. on Advances in Signal Processing*, Jan. 2011.
- [14] L. Chen, R. Nie, Y. Chen, and W. Wang, “Hierarchical-absolute reciprocity calibration for millimeter-wave hybrid beamforming systems,” *IEEE Transactions on Wireless Communications*, 2022.
- [15] B. M. Lee, “Calibration for channel reciprocity in industrial massive MIMO antenna systems,” *IEEE Transactions on Industrial Informatics*, vol. 14, no. 1, pp. 221–230, 2017.
- [16] X. Jiang, M. Ćirkić, F. Kaltenberger, E. G. Larsson, L. Deneire, and R. Knopp, “MIMO-TDD reciprocity under hardware imbalances: Experimental results,” in *IEEE International Conference on Communications (ICC)*, 2015, pp. 4949–4953.
- [17] X. Luo, F. Yang, and H. Zhu, “Massive MIMO self-calibration: Optimal interconnection for full calibration,” *IEEE Transactions on Vehicular Technology*, vol. 68, no. 11, pp. 10 357–10 371, 2019.
- [18] H. Papadopoulos, O. Y. Bursalioglu, and G. Caire, “Avalanche: Fast RF calibration of massive arrays,” in *IEEE GlobalSIP*, 2014.
- [19] X. Jiang, A. Decurninge, K. Gopala, F. Kaltenberger, M. Guillaud, D. Stock, and L. Deneire, “A framework for over-the-air reciprocity calibration for TDD massive MIMO systems,” *IEEE Transactions on Wireless Communications*, vol. 17, no. 9, pp. 5975–5990, 2018.
- [20] R. Rogalin, O. Y. Bursalioglu, H. Papadopoulos, G. Caire, A. Molisch, A. Michaloliakos, V. Balan, and K. Psounis, “Scalable synchronization and reciprocity calibration for distributed multiuser MIMO,” *IEEE Trans. Wireless Commun.*, vol. 13, no. 4, pp. 1815–1831, Apr. 2014.
- [21] J. Vieira and E. G. Larsson, “Reciprocity calibration of distributed massive MIMO access points for coherent operation,” in *IEEE PIMRC*, 2021.
- [22] C.-M. Chen, S. Blandino, A. Gaber, C. Desset, A. Bourdoux, L. Van der Perre, and S. Pollin, “Distributed massive MIMO: A diversity combining method for TDD reciprocity calibration,” in *Proc. of IEEE GLOBECOM*, 2017.
- [23] N.-I. Kim, C. W. Yu, S.-E. Hong, J.-H. Na, and B. C. Chung, “A gradual method for channel non-reciprocity calibration in cell-free massive MIMO,” *IEEE Communications Letters*, vol. 26, no. 11, pp. 2779–2783, 2022.
- [24] Y. Cao, P. Wang, K. Zheng, X. Liang, D. Liu, M. Lou, J. Jin, Q. Wang, D. Wang, Y. Huang *et al.*, “Experimental performance evaluation of cell-free massive MIMO systems using COTS RRU with OTA reciprocity calibration and phase synchronization,” *IEEE Journal on Selected Areas in Communications*, pp. 1620–1634, 2023.
- [25] H. V. Balan, R. Rogalin, A. Michaloliakos, K. Psounis, and G. Caire, “AirSync: Enabling distributed multiuser MIMO with full spatial multiplexing,” *IEEE/ACM Transactions on Networking*, vol. 21, no. 6, pp. 1681–1695, 2013.
- [26] M. Rashid and J. A. Nanzer, “Frequency and phase synchronization in distributed antenna arrays based on consensus averaging and Kalman filtering,” *IEEE Transactions on Wireless Communications*, pp. 2789–2803, 2023.
- [27] U. K. Ganesan, R. Sarvendranath, and E. G. Larsson, “BeamSync: Over-the-air synchronization for distributed massive MIMO systems,” *IEEE Transactions on Wireless Communications*, 2023.
- [28] R. Nissel, “Correctly modeling TX and RX chain in (distributed) massive MIMO – new fundamental insights on coherency,” *IEEE Communications Letters*, pp. 2465–2469, Oct. 2022.
- [29] H. M. Aumann, A. J. Fenn, and F. G. Willwerth, “Phased array antenna calibration and pattern prediction using mutual coupling measurements,” *IEEE Transactions on Antennas and Propagation*, vol. 37, no. 7, pp. 844–850, 1989.

- [30] J. Vieira, F. Rusek, and F. Tufvesson, "A receive/transmit calibration technique based on mutual coupling for massive MIMO base stations," in *Proc. of IEEE PIMRC*, 2016.
- [31] O. Simeone, U. Spagnolini, Y. Bar-Ness, and S. H. Strogatz, "Distributed synchronization in wireless networks," *IEEE Signal Processing Magazine*, vol. 25, no. 5, pp. 81–97, 2008.
- [32] Y.-C. Wu, Q. Chaudhari, and E. Serpedin, "Clock synchronization of wireless sensor networks," *IEEE Signal Processing Magazine*, vol. 28, no. 1, pp. 124–138, 2010.
- [33] A. Arenas, A. Díaz-Guilera, J. Kurths, Y. Moreno, and C. Zhou, "Synchronization in complex networks," *Physics Reports*, vol. 469, no. 3, pp. 93–153, 2008.
- [34] D. Ghosh, M. Frasca, A. Rizzo, S. Majhi, S. Rakshit, K. Alfaro-Bittner, and S. Boccaletti, "The synchronized dynamics of time-varying networks," *Physics Reports*, vol. 949, pp. 1–63, 2022.
- [35] F. Dörfler and F. Bullo, "Synchronization in complex networks of phase oscillators: A survey," *Automatica*, vol. 50, no. 6, pp. 1539–1564, 2014.
- [36] M. Lucas, G. Cencetti, and F. Battiston, "Multiorder Laplacian for synchronization in higher-order networks," *Physical Review Research*, vol. 2, no. 3, 2020.
- [37] C. Godsil and G. F. Royle, *Algebraic Graph Theory*. Springer, 2001.
- [38] R. A. Horn and C. R. Johnson, *Matrix Analysis*. Cambridge University Press, 1999.
- [39] D. Gesbert, M. Kountouris, R. W. Heath, C.-B. Chae, and T. Salzer, "Shifting the MIMO paradigm," *IEEE Signal Processing Magazine*, vol. 24, no. 5, pp. 36–46, 2007.
- [40] E. Björnson, M. Bengtsson, and B. Ottersten, "Optimal multiuser transmit beamforming: A difficult problem with a simple solution structure," *IEEE Signal Processing Magazine*, vol. 31, no. 4, pp. 142–148, 2014.
- [41] D. M. Cvetković, M. Doob, and H. Sachs, *Spectra of Graphs: Theory and Applications*. Academic Press, 1980.
- [42] R. M. Gray, "Toeplitz and circulant matrices: A review," *Foundations and Trends® in Communications and Information Theory*, vol. 2, no. 3, pp. 155–239, 2006.
- [43] W. Zhang and Y. Jiang, "Over-the-air phase calibration of reconfigurable intelligent surfaces," *IEEE Wireless Communications Letters*, 2023.
- [44] S. Hu, F. Rusek, and O. Edfors, "Beyond massive MIMO: The potential of data transmission with large intelligent surfaces," *IEEE Transactions on Signal Processing*, vol. 66, no. 10, pp. 2746–2758, 2018.
- [45] B. Mohar, "Eigenvalues, diameter, and mean distance in graphs," *Graphs and Combinatorics*, vol. 7, no. 1, pp. 53–64, 1991.
- [46] N. M. M. De Abreu, "Old and new results on algebraic connectivity of graphs," *Linear Algebra and its Applications*, vol. 423, no. 1, pp. 53–73, 2007.